外科に応用できると思います．

あと外科的な面では，例えば**静脈の温存**も検討したいと思います．現在は，「静脈梗塞を起こしたんだろう」という推察で話が終わってしまい，Contusionかどうかわからない．静脈の状態，この静脈は温存すべきか，やむを得ないときはsacrificeできるのかどうかとかという，静脈還流と脳のダメージの具合もICG flowmeter等を用いて可視化できれば，手術するうえで有用だと思いますね．

9 Future direction：Brain-machine interface

【川原】Brain-machine interfaceについてはどのようにお考えですか？　病気などで機能を失った人の機能再建に，先生の研究が役立ってこようかと思いますが．

【鎌田】20年経つとmodalityが変わります．今は脳波を使っていますが，近赤外線もありますね．基本的な学問として解読手法，基礎があれば，あとは工学系のほうでデバイスが開発されれば，それに応用できるはずです．だから，何をやるにしても右手を出せば次は左手というように，少しずつ，1歩1歩学問が進んでいくので，どこかで何かが進むときに自分がそれに遅れないように，**常にその先端にいて，今，何が使えるものかと見ていくことが大事**だと思います．

10 脳神経外科医としての使命

【川原】先生の今までの研究や臨床でのご経験から，若い人たちに何かメッセージをお願いします．

【鎌田】まずは，**なぜ脳神経外科医になったか，それを思い出してほしい**と思いますね．忙しいルーチンのなか，みなさん頑張ってやっていると思うんですが，何をやりたくてこの仕事をしているのかを思い返してほしいと思います．

【川原】脳神経外科を選んだ原点にかえるということですね．

【鎌田】はい．僕が工学部に行ったのもそうなんですが，当然，日々の忙しさもあるけれども，なぜなりたかったかということを思い出して，それを目指してほしいと思います．

また，まず**患者の痛みを知ってほしい**と思います．いくら志を高く持って手術しても，全部うまくいくわけではないですね．やはり，痛い目に遭うときもあると思うんです．でも，うまくいかなかった場合にもきちんとそれに向き合って，何がこの患者さんの手術で悪かったのか画像も舐めるように見て，出た症状や患者さんのつらかったこと，それをしっかり直視して，1例見たら絶対忘れないで，二度と同じ轍を踏まないように頑張る．それが医学の進歩につながるし，医師としての自分の進歩にもつながると思います．

常にその先端にいて，今，何が使えるものか見ていくことが大事．

「光明を照らせる人になりたくないか？」

11 私を突き動かすもの

【川原】先生は研究も臨床も，ずっと没頭してやってきたということでしたが，それは性格もあるのでしょうが，そのように自分を突き動かしてきた力，driving force は何だと思いますか？

【鎌田】2年目か3年目に上山博康先生に言われた言葉が今でも忘れられません．**「光明を照らせる人になりたくないか？ どの分野でも，どんな狭い分野でもいいから，プロフェッショナルになれ」**と．それを胸に刻んで，どの分野に行っても，与えられた場で精一杯，努力してきました．

【川原】そういうモチベーションを維持していくことが大事だということですね．

【鎌田】はい．あとは，**仲間，そして環境を大切にする**ということですね．誰しもそうだと思うんですが，外科医である限り，手術がやりたいし，そのスキルを磨きたい．でも，自分が手術できないときもやはりあるわけです．僕が自分に言い聞かせたのは，「自分が悪いんだ」ということです．できない自分が悪い．その立場にいない自分が悪い．なので，それならそれで，そこでできることをやろうと思うんですね．そうすると，急にチャンスが来たときでも準備していればできるはずなので，自分が置かれた環境で精一杯，周りと一緒に仲良くやっていって，周りをサポートする．そうすると，気付かないうちに周りからもサポートが得られる．これはいくつかの大学を経たことと，いろいろな国に留学して学んだことです．「早く手術がしたい」と思っている若手も多いかもしれませんが，いつ手術ができるようになるかはタイミングもあるので，その機会がきたときにできるように準備していないと駄目だと思いますね．

【川原】そのとおりだと思います．その準備というのは，上司や部下を含めた同僚とのいろいろなコミュニケーションのなかから情報を集めることも含むということですね．万端な準備をしておけ，物事を焦るな，かならずチャンスは巡ってくる，ということでしょうか．

【鎌田】そのとおりです．

【川原】今日は貴重なお話をお聞かせいただき，ありがとうございました．

インタビューを終えて

今回の鎌田先生との対談「脳機能の可視化への挑戦」では，たいへん勉強させていただきました．鎌田先生は，ドイツ，米国と2カ国に留学され，「脳機能の可視化」に世界レベルで早期から研究に取り組んでこられました．「今のことに没頭する」姿勢が，現在は世界レベルで研究されている仕事につながっているものと思います．現在の卒後研修のなかでは，2～3年先のことばかりが気になってしまい，逆に没頭することが「怖い」と思っている方も多く見受けられます．20～30年先を見つつ今に没頭することが，明日への展開となることがよくわかりました．

脳の形は見えても機能は見えませんでしたが，脳の大切さは機能にあることは疑いの余地がありません．現在は医工学の発展により実際の手術の現場でも見えるようになってきましたが，その背景には鎌田先生のような研究者の努力があることを，改めて感じた次第です．

一方で，鎌田先生は卓越した技量を持つ外科医でもあります．今後の臨床，研究の発展をお祈りすると同時に，若い読者の先生方には，「没頭する」ことを恐れずに果敢に挑戦する気持ちをぜひとも学んでいただきたいと思います．（川原信隆）

Biocybernetics and Biomedical Engineering
2011, Volume 31, Number 2, pp. 33–50

Multimodal Neurosurgery Force Feedback System Based on Mesh Fusion Modeling

YOSHIHIRO KURODA[1,*], KYOUSUKE KAMADA[2], YOSHIMITSU HAYASHI[2], MASATAKA IMURA[1], OSAMU OSHIRO[1]

[1] *Graduate School of Engineering Science, Osaka University, Japan*
[2] *School of Medicine, Asahikawa Medical University, Japan*

Virtual reality based force feedback system is spotlighted as a safe and efficient training environment to obtain surgical skills. Neurosurgery utilizes multimodal patient images for visualization of a variety of functions in head. The aim of this study is to establish a concept of multimodal neurosurgery force feedback system based on mesh fusion modeling. In the model of mesh fusion, we developed an algorithm to detect overlapped region between the multiple meshes that are obtained from multimodal images, and to determine a new boundary between the meshes. Then, the method solved interaction between the newly defined mesh boundaries using the interaction model based on a finite element method. The proposed method was implemented, and applied to both simple and patient datasets for evaluating its applicability. As a result, the method succeeded to be applied to both simple and patient datasets. Finally, we demonstrated the early stage of the surgical approach in neurosurgery. Simulation results showed a real-time simulation of brain tissue deformation with force feedback.

K e y w o r d s: virtual reality, surgical simulation, neurosurgery, finite element method, haptics

1. Introduction

Information technologies have made a great progress and increased possibility of a virtual reality (VR) based surgical simulation system for the purpose of training, pre-planning, and intra-operative support [1]. The surgical simulator simulates the physical behavior of human body and artificially stimulates human senses to create

* Correspondence to: Yoshihiro Kuroda, Graduate School of Engineering Science, Osaka University, Japan, e-mail: ykuroda@bpe.es.osaka-u.ac.jp
Received 30 December 2010; accepted 08 February 2011

an experience similar to one gained by a surgeon treating of a real patient. In surgical simulation, not only fidelity but also interactivity of physics simulation are required for visual and haptic feedback in response to a user's action. Recently, real-time simulation of physics-based tissue deformation is reported from several research groups. Sorensen applied the General Purpose Graphics Processing Unit (GPGPU) approach to a real-time spring-mass based deformation of heart for cardiac surgery simulation [2]. Kuroda simulated liver deformation using a finite element method (FEM) with the multi-finger force display [3]. Bachofen improved realism of the Hysteroscopic VR system by blood flow simulation [4].

In neurosurgery, surgeon treats fine structures in the skull with delicate force control without damaging small vessels and nerves. Recent advances in measurement methods enable detection of the fine brain structures [5]. Since the measurement methods to detect brain substances and vessels are different, the surgeon must integrate multimodal 3D images to observe the geometrical relationship of the brain structures. Surgical simulation also has to consider complicated structures obtained by multimodal images to improve realism of the simulation. Neurosurgery simulation with sole modality is less practical because the detailed structures of vessels and nerves are obtained from multimodal images. Surgical simulation has been studied as related to neurosurgery as well as other surgical fields [6–9]. For example, Hayashi proposed a system to navigate a target lesion, and Spicer proposed a simulator with multi-modality images [7]. However, the systems have never taken into consideration the force feedback and collisions of the simulated objects (i.e., meshes) as obtained from the multimodal images. Kuroda proposed a concept of neurosurgery force feedback system [10, 11]. The paper, however, focused on describing a concept of the proposed framework, and introduced an approach to solve the problem briefly [10]. On the other hand, the other paper applied an algorithm only to simple objects, not to patient datasets [11].

The aim of this study is to establish a multimodal neurosurgery force feedback system for the purpose of surgical training, pre-planning and intra-operative navigation. This paper proposes a mesh fusion model allowing multimodal brain data to use in neurosurgery simulation, describes details of the algorithm, and demonstrates the effect of the model by using not only simple but also patient datasets.

In FEM, the geometry of objects is represented as a large number of tetrahedral elements. The boundary and mechanical properties are set on each element. The set of elements are called mesh. The multiple meshes are obtained from multimodal images. Spatial overlap among the meshes requires consideration of the treatment of the overlapped regions and the mesh-mesh interaction. The proposed algorithm proceeds overlapped region between the meshes and allows interaction between the meshes by using the model of interaction between the meshes [12]. In this paper, the mesh consists of a set of tetrahedral elements to represent complicated geometry of human tissue.

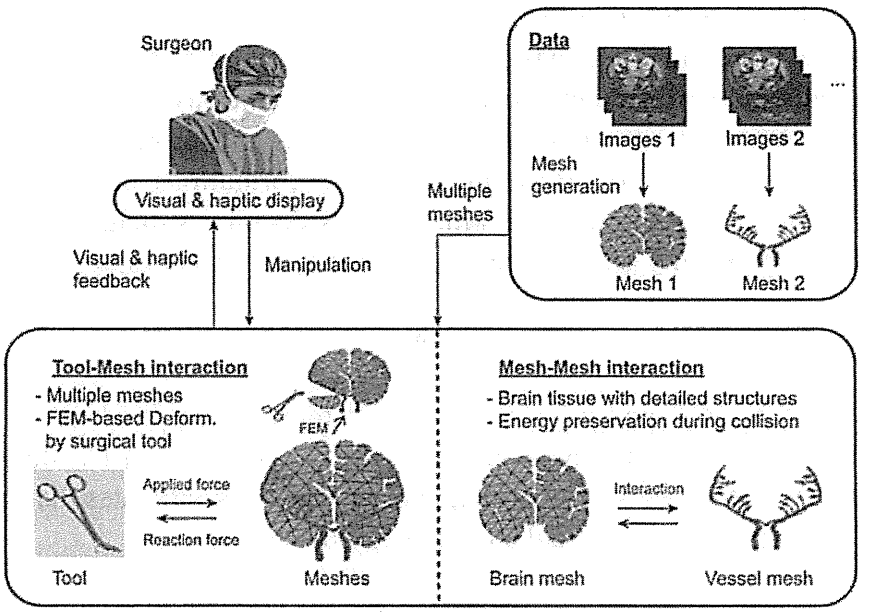

Fig. 1. Concept of multimodal neurosurgery force feedback system based on mesh fusion modeling

2. Methodology

2.1. Concept

Figure 1 illustrates the concept of the multimodal neurosurgery force feedback system, which consists of the following functions:

1. Tool-mesh interaction with visual and haptic feedback
2. Mesh-mesh interaction
3. Visualization of deformed volumetric images

The multiple meshes for simulation are obtained from the sets of 3D images. The system measures surgeon's manipulation and updates the position of a virtual tool, i.e. surgical instrument. The mesh, i.e. tissue model, is deformed by FEM if the collision between the mesh and the tool is detected. The interaction between the meshes is considered in order to enhance accuracy and realism of the simulation. The reaction force is calculated and fed back to the user.

Figure 2 shows all procedures of the proposed simulation framework. The methods of inclusion processing and FEM with mesh interaction are described in this section.

2.2. Modeling Deformation

Physically-based deformable modeling has been widely studied [12, 13, 14]. The FEM-based model treats an object as continuum and has an advantage over simple mass-spring networks. In general, the FEM based analysis requires much computation

to solve simultaneous differential equations. If an object has N nodes that have three degrees of freedom, the model has $3N$ degrees of freedom and requires solution of $3N$-sized simultaneous differential equations. Thus, in the past it was mainly used in off-line computation. However, the growth in computer and information technologies enabled real-time calculation of the FEM-based deformations. In this study, FEM is applied to the deformation of the brain and its detailed structures. FEM yields a stiffness matrix, **K**, and relates displacements to applied forces.

$$\mathbf{f} = \mathbf{K}\mathbf{u} \tag{1}$$

where $\mathbf{f} = (f_1\ f_2\ \ldots\ f_n)^{\mathrm{T}}$ and $\mathbf{u} = (u_1\ u_2\ \ldots\ u_n)^{\mathrm{T}}$ represent applied forces and displacements, respectively, and **K** is an n by n stiffness matrix. Eq.1 is derived from the principle of virtual work. The principle of virtual work indicates that the virtual work by force equals to the virtual strain energy by stress.

$$\mathbf{U} - \mathbf{W} = \mathbf{0} \tag{2}$$

where **U**, **W** represent virtual strain and virtual work, respectively. The energy conservation is applied to the mesh-mesh interaction as well.

2.3. Modeling Mesh-mesh Interaction

Interaction between objects occurs when the objects collide with each other. If energy is not lost during the collision, total energy of the two objects is preserved.

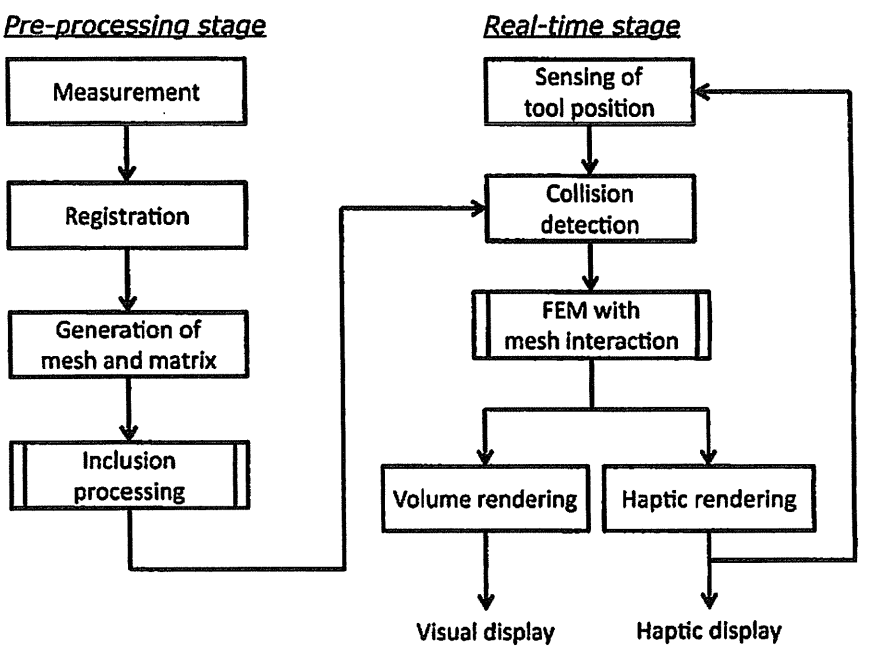

Fig. 2. Procedures of the multimodal neurosurgery force feedback system

The work by applied force is stored as strain energy. Now, we assume that a tool pushes or pulls one of the two objects, and the collision between the objects occurs as shown in Fig. 3. Figure 3(a) and Figure 3(b) show inclusion and non-inclusion types, respectively. The visualization of deformed volumetric data is realized by sliced-based volume rendering for real-time and high quality visualization. The volumetric data is reconstructed from the slices obtained by measurement methods, e.g. Magnetic Resonance Imaging (MRI) and X-ray Computed Tomography (CT).

2.4. Inclusion Processing

If multiple meshes exist in a space, the spatial relationship between the multiple meshes can be categorized into two types as shown in Figure 3. Figure 3(a) has no overlapped region between the meshes, while Figure 3(b) has the overlapped region.

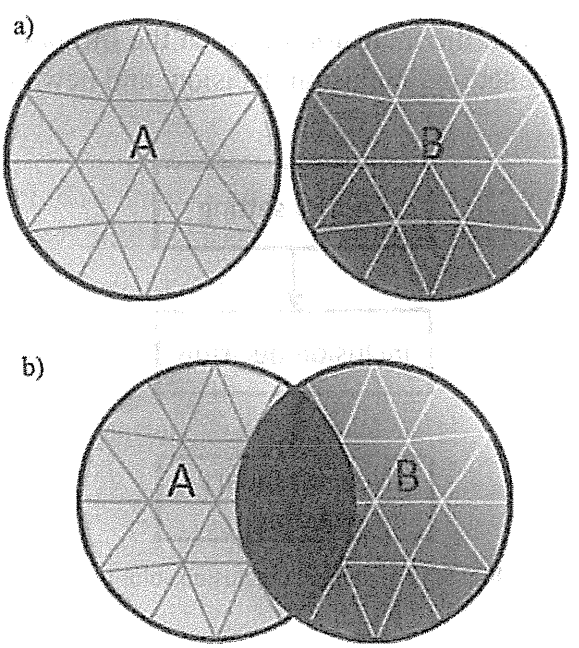

Fig. 3. Inclusion relationship between multiple meshes: a) no overlapped region exits, b) an overlapped region exists

Figure 4(a) illustrates the case of no overlapped region between the meshes. If there is no spatial overlap between the meshes, mechanical properties represented by each mesh are utilized for physical simulation. The work by applied forces is stored as strain energy of meshes. Figure 4(b) illustrates the case of an overlapped region between meshes.

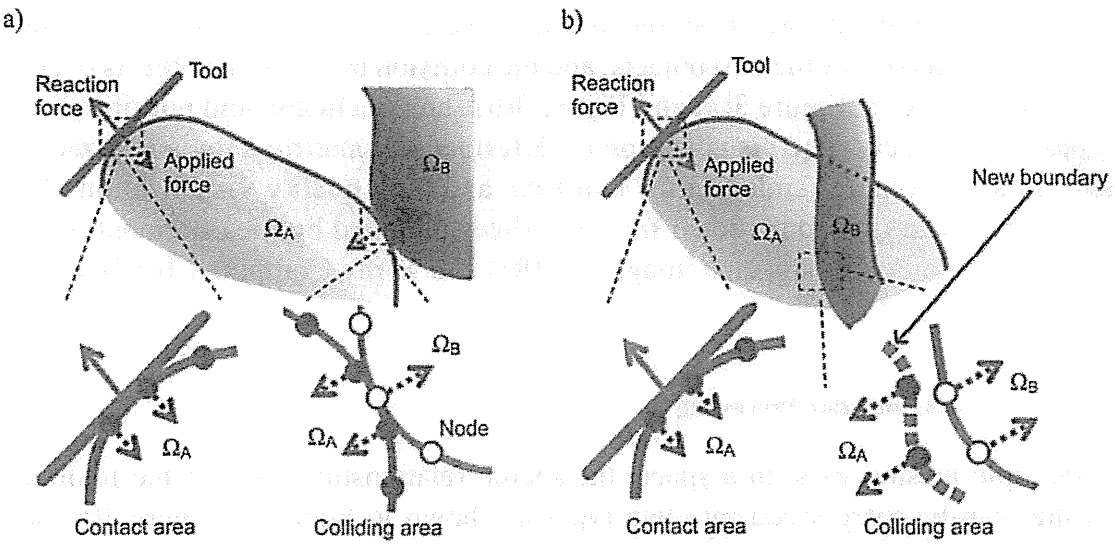

Fig. 4. Spatial representation and interaction between the multiple meshes: (a) the case of no overlapped region and (b) the case of an overlapped region, where Ω_A, Ω_B are the regions of the objects A and B, respectively

As shown in Figure 5, the inclusion between the meshes is treated as the following process: priority setting, inclusion decision, and new boundary setting.

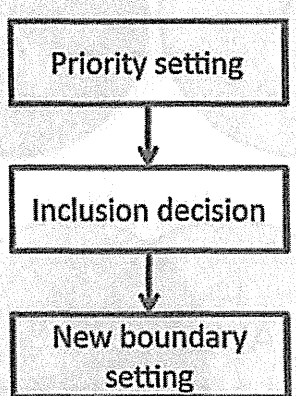

Fig. 5. Procedures in inclusion solution

If there is a spatial overlap between the meshes, the priority between the meshes is set for the overlapped region to represent the mechanical properties in the space properly.

The mesh that is obtained for fine vessel structure represents the property in the space properly. For example, if the mesh of brain substance by MRI imaging (called brain mesh below) has any overlapped region with the mesh of vessel (called vessel mesh below), the vessel mesh represents the functional structure in the space in comparison with the brain mesh. Hence, in this case, the priority of the vessel mesh is set higher than the brain mesh.

Next, new boundary is defined, if the overlapped region exists. As a result, the work of the force applied by the user is stored as strain energy of both colliding meshes through the new defined boundary. The alternative way is the reconstruction of meshes to remove the overlapped region, instead of setting a new boundary. However, this solution is computationally expensive. This study takes an approach of setting a new boundary.

2.5. Algorithm

In this section, we describe how to define a new boundary with the colliding meshes. Here, inclusion relationship of the meshes A and B is examined. Concretely, the triangles of the mesh A in the tetrahedron that has intersected triangles with the surface triangles of the mesh B are registered as a possible new boundary, if the triangles are outside the mesh B. Figure 6 illustrates the elements intersected between the meshes A and B in two dimensions, and the new boundary defined by the algorithm. In this study, geometrical reconstruction of removing the overlapped region from the mesh A is not carried out, under the assumption that a small mesh representing fine structures, such as vessels and nerves, is located inside a large mesh representing brain substance, and then the effect of the overlapped region in the mesh A is small.

The description and pseudo code of the algorithm for inclusion decision are described below.

1. Priority is set on a pair of meshes. Here, the priority of the mesh B is set higher than that of the mesh A.
2. Intersection detection of the bounding box of the meshes A and B checks possibility of intersection between the meshes. If no intersection is found,

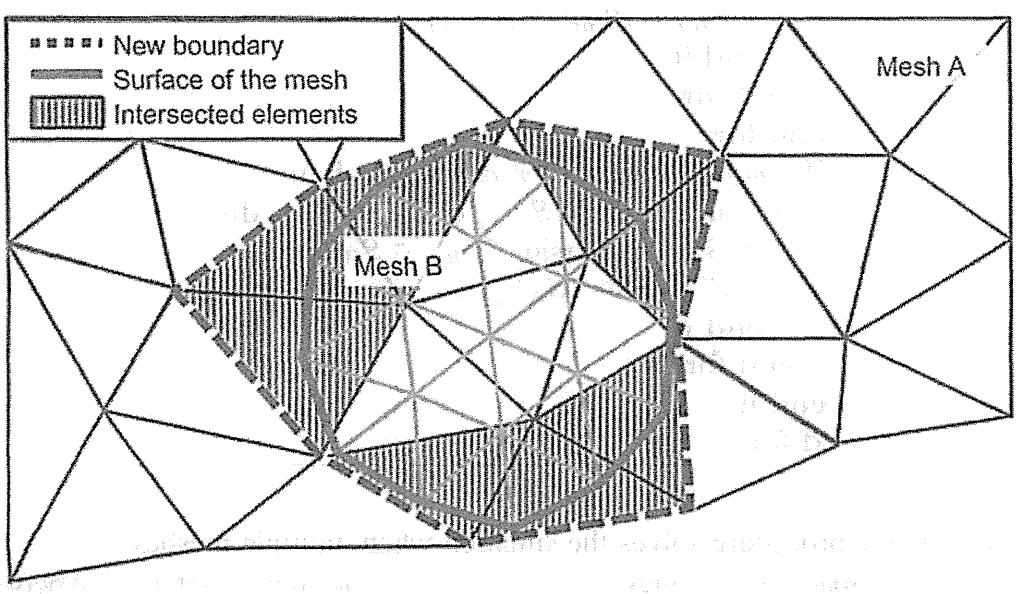

Fig. 6. Intersected elements and a new boundary between the meshes A and B

the processing goes to the step 5. If intersection is found, then the processing goes to the step 3 for detail checking.

3. Intersection detection between triangles of a tetrahedral element $T_{A,i}$ and all surface triangles of the mesh B is carried out. If no intersection is found or all triangles of the tetrahedral element are intersected, the processing goes to the step 5. Otherwise, the processing goes to the step 4.
4. The non-intersected triangles of the tetrahedral element $T_{A,i}$ are added to the triangles of the new boundary if the triangles are outside all surface triangles of the mesh B.
5. The processing goes to the step 3 until all tetrahedral elements of the mesh A are processed.

Algorithm 1 Inclusion decision

Input: The set of tetrahedral elements of mesh A: $T_A = \{T_{A,0}, T_{A,1}, \ldots, T_{A,n-1}\}$ and the set of surface triangles of mesh B: $S_B = \{S_{B,0}, S_{B,1}, \ldots, S_{B,m-1}\}$.
Output: The set of new boundary triangles of mesh A: $S' = \{S'_0, S'_1, \ldots, S'_{l-1}\}$.

```
count_max ← 4
S' ← ∅
for each tetrahedral element T_{A,i} of mesh A do
  count ← 0
  S_int ← ∅
  for each triangle S_{A,i,j} of T_{A,i} do
    for each surface triangle S_{B,k} of mesh B do
      if S_{A,i,j} intersects with S_{B,k} then
        count ← count + 1
        S_int ← S_int + {S_{A,i,j}}
      end if
    end for
  end for
  if count ≠ 0 ∧ count ≠ count_max then
    for each triangle S_{A,i,j} of T_{A,i} ∉ S_int do
      if S_{A,i,j} is outside ∀S_{B,k} ∈ S_B then
        S' ← S' + {S_{A,i,j}}
      end if
    end for
  end if
end for
```

The above procedure solves the situation when multiple meshes overlap with each other in a space, and defines a new boundary to consider the interaction between the meshes.

2.6. Simulation of Contact Deformation

The contact deformation between meshes is solved by the interaction model proposed in [12]. The interaction model yields virtual displacement to colliding meshes, and determines displacements of the meshes to minimize the difference of virtual stresses by using Eq. 3. As related studies, Selle proposed a method, which yields a constraint of preserving the relative velocity before and after collision of bodies [15]. However, the method never determines any contact deformation occurred in collision. Sibille and Joukhadar proposed methods to determine displacements of colliding meshes based on geometrical information, such as the barycenter and volume of the overlapped region, respectively [16, 17]. The methods, however, never take into consideration the different stiffness of two objects. On the other hand, the interaction model proposed in [12] takes into account the contact stress of colliding objects. As a result, the model represents the contact deformation that reflects mechanical properties.

The difference of virtual stress between meshes i, j is represented as

$$|\mathbf{E}_{i,j}| = |\boldsymbol{\sigma}_i(\mathbf{u}_i) - \boldsymbol{\sigma}_j(\mathbf{u}_j)| \tag{3}$$

where $\mathbf{u}_i, \mathbf{u}_j$ are virtual displacements in the mesh i and j, respectively, and $\boldsymbol{\sigma}_i$, $\boldsymbol{\sigma}_j$ are virtual stresses in the mesh i and j, respectively. The iteration process yields displacements $\mathbf{u}_i, \mathbf{u}_j$ by minimizing $|\mathbf{E}_{i,j}|$.

Computational cost of real-time processing to calculate the deformation and force can be reduced by preprocessing [18]. The displacement is calculated by using the inverse of the stiffness matrix $\mathbf{L} = \mathbf{K}^{-1}$ as shown in Eq. 4.

$$\mathbf{u} = \mathbf{L}\mathbf{f}. \tag{4}$$

In Figure 4, the nodes in the mesh A are categorized into the following three types: contact nodes by a user, colliding nodes with the mesh B and the other nodes. The nodes in the mesh B are categorized into the following two types: colliding nodes with the mesh A and the other nodes. The stiffness equations of objects A and B are as follows:

$$\begin{pmatrix} \mathbf{u}_c \\ \mathbf{u}_b \\ \mathbf{u}_o \end{pmatrix} = \begin{pmatrix} \mathbf{L}_{cc} & \mathbf{L}_{cb} & \mathbf{L}_{co} \\ \mathbf{L}_{bc} & \mathbf{L}_{bb} & \mathbf{L}_{bo} \\ \mathbf{L}_{oc} & \mathbf{L}_{ob} & \mathbf{L}_{oo} \end{pmatrix} \begin{pmatrix} \mathbf{f}_c \\ \mathbf{f}_b \\ \mathbf{f}_o \end{pmatrix} \tag{5}$$

$$\begin{pmatrix} \mathbf{u}'_b \\ \mathbf{u}'_o \end{pmatrix} = \begin{pmatrix} \mathbf{L}'_{bb} & \mathbf{L}'_{bo} \\ \mathbf{L}'_{ob} & \mathbf{L}'_{oo} \end{pmatrix} \begin{pmatrix} \mathbf{f}'_b \\ \mathbf{f}'_o \end{pmatrix} \tag{6}$$

where subscripts c, b, o represent nodes in contact with a user, colliding boundary nodes between the meshes and the other nodes, respectively. The displacements of

both objects are calculated by the interaction model proposed in [12]. The user's input is given as the displacement $\mathbf{u}_c$. Not applying force on the contact and boundary nodes yields $\mathbf{f}_o = \mathbf{f}'_o = \mathbf{0}$. Virtual forces $\mathbf{f}_b$, $\mathbf{f}'_b$ are calculated, when virtual displacement $\mathbf{u}_b$, $\mathbf{u}'_b$ are given in the colliding boundary nodes. The interaction model yields $\mathbf{u}_b$, $\mathbf{u}'_b$. Finally, reaction force and deformation are calculated from $\mathbf{f}_c$, $\mathbf{u}_o$, $\mathbf{u}'_o$. Slice-based volume rendering and the mapping of 3D texture to deformed geometry of the meshes enabled volume deformation with 3D texture [19].

3. System and Data

The system was developed for evaluation. Table 1 shows the specification of the system. Figure 7 shows the outlook of the system. We prepared a simple-shaped model and a patient model. The simple-shaped model used cubic and cylindrical objects as shown in Fig. 8. The patient model consisted of the brain substance and an artery as shown in Fig. 9. The components of the model are shown in Table 2. MRI volumetric data is reduced to 256 × 256 × 256 in size, and used for volume texture. Amira by Mercury Inc., is used for mesh generation. Mechanical properties of the brain are reported by a lot of studies. In this study, we applied 1.0MPa in Young modulus and 0.4 in Poisson's ratio to the model, which parameters are within the living tissue.

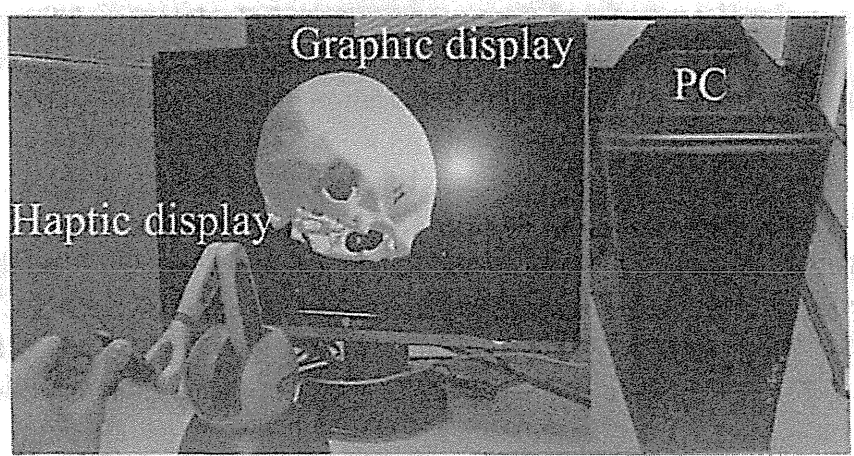

Fig. 7. System overview

Table 1. System specification

Item	Name
CPU	Intel Core2 Extreme 3.0GHz (4 core)
Main memory	6.0GB
Graphic board	nVidia GeForce 8800GT
Graphic display	LCD monitor
Haptic display	SensAble PHANToM Omni

Table 2. Model components: (a) simple-shaped model, (b) patient model

a)

	Cube	Cylinder
Vertices	1812	206
Tetrahedron	8324	699
Young modulus[MPa]	1.0	0.1

b)

	Brain substance	Artery
Vertices	5367	1644
Tetrahedron	25103	4449

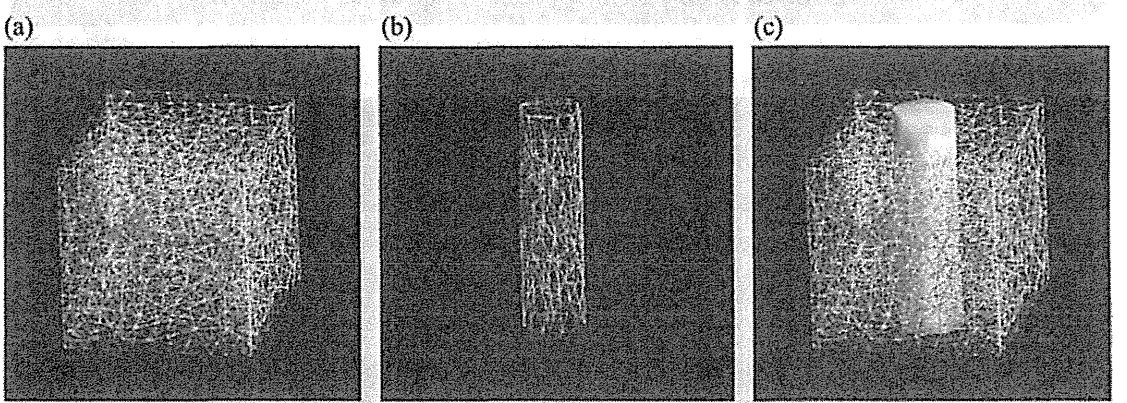

Fig. 8. Simple objects: (a) cube, (b) cylinder, (c) cylinder placed in the cube

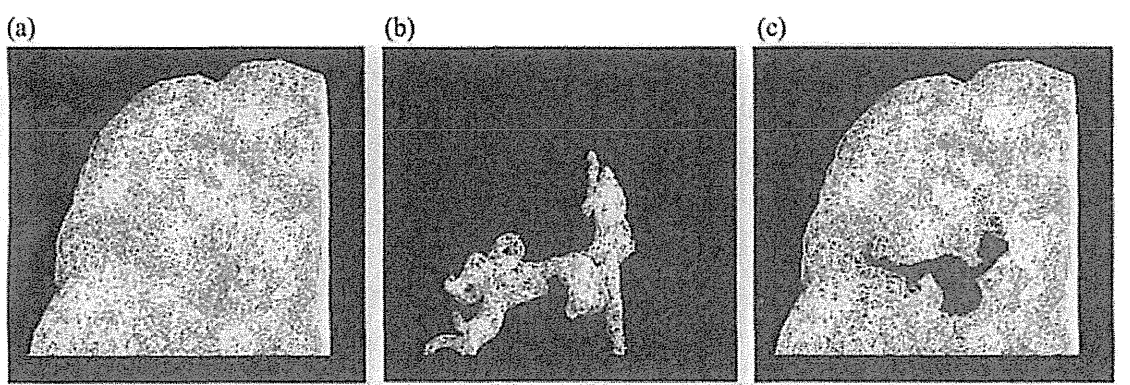

Fig. 9. Brain-artery objects: (a) brain substance, (b) artery, (c) artery placed in the brain substance

Figure 10 shows the result of applying the method to the cubic and cylindrical meshes. The cylindrical mesh was placed in the cubic mesh. As the overlapped region between the meshes existed, a new boundary was defined by the proposed algorithm. User pushes the cubic mesh from right to left. Figure 10 (a-c) shows the result without consideration of interaction between the meshes. No deformation of

the cylindrical mesh was found. Figure 10 (d-i) shows deformation with consideration of interaction between the meshes. The deformation of the cylindrical mesh was found.

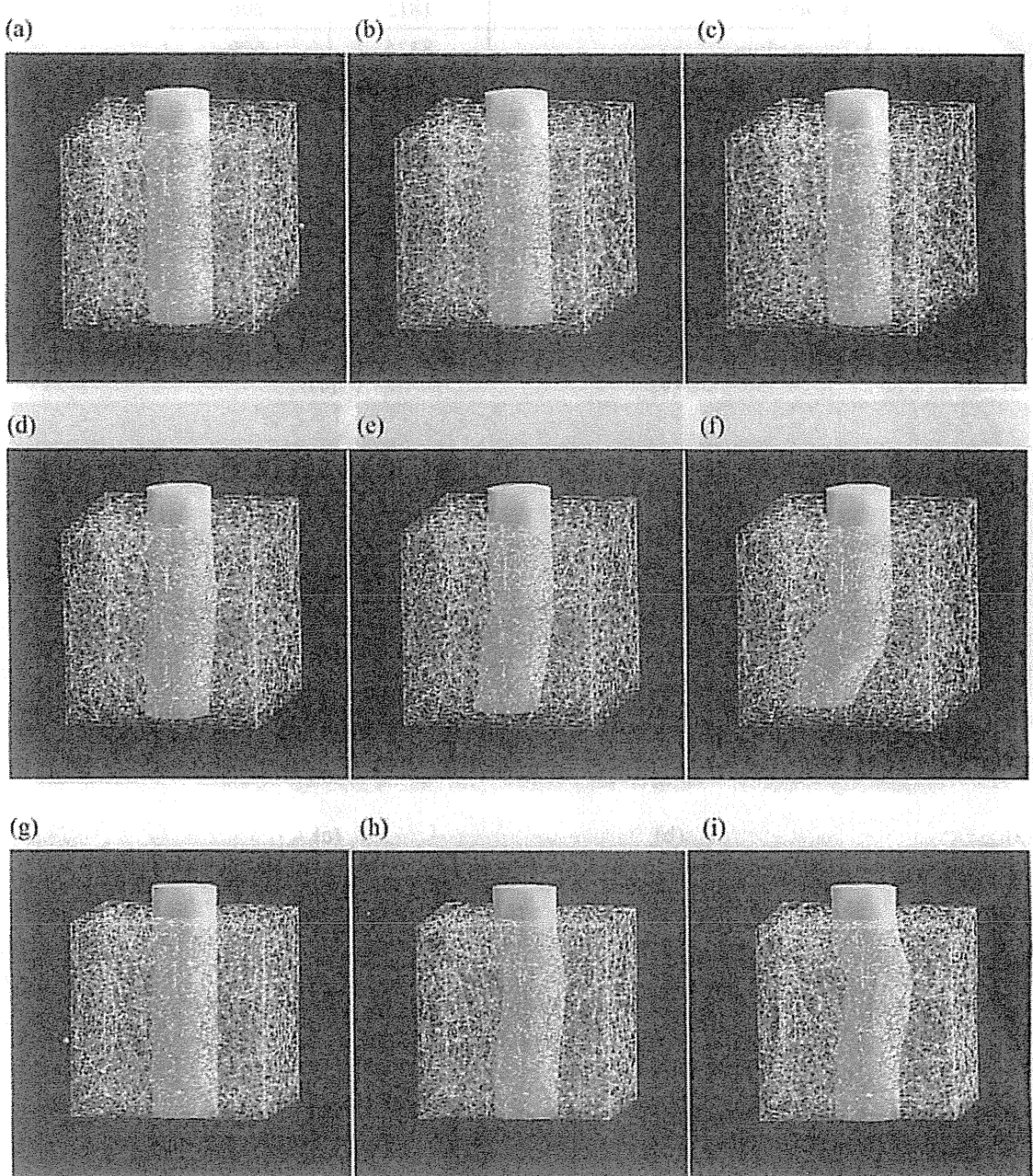

Fig. 10. Simulation result in the case of a simple object: (a–c) deformation without consideration of the mesh-mesh interaction, (d–f) deformation by pushing the cubic mesh from the right side and (g–i) from the left side with consideration of the mesh-mesh interaction

The new boundaries defined with the simple-shaped models are shown in Fig. 11. The new boundaries have non-flat surface, because the boundaries have been collected from the inner triangles of the mesh. However, the result showed that the smoothness

of the new boundaries increased as number of vertices of the mesh increased. The new boundary defined with the patient model is shown in Fig. 12. The algorithm succeeded to define the new boundary surrounding around the artery mesh.

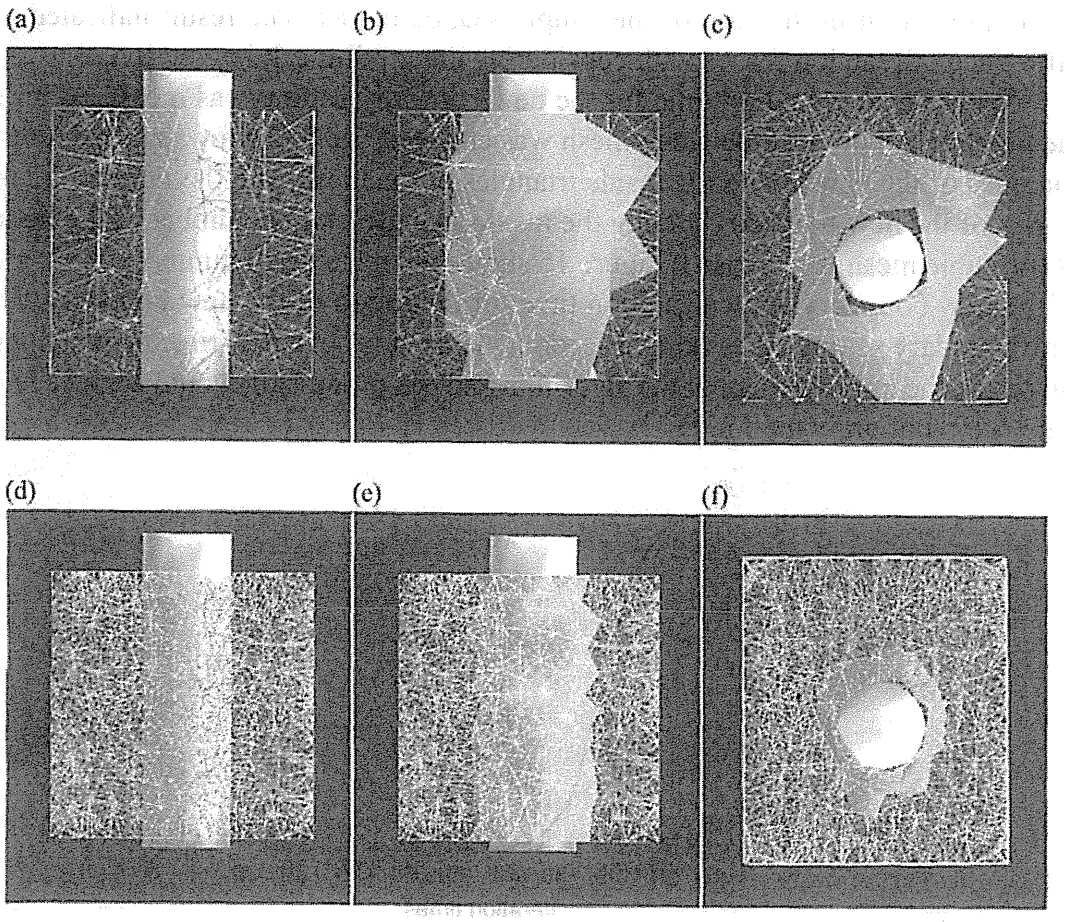

Fig. 11. New defined boundaries with the simple-shaped models with 195 and 1521 vertices: (a, d) meshes, (b, e) front view, (c, f) upside view

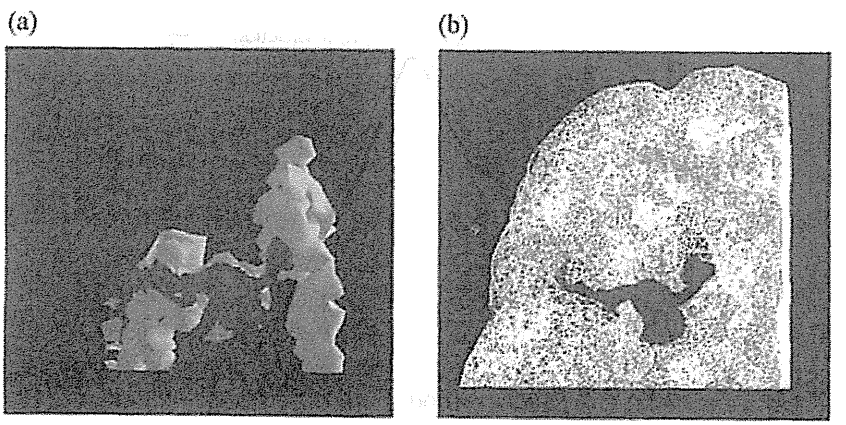

Fig. 12. New defined boundary with the patient model: (a) artery and new boundary, (b) brain substance, artery and new boundary

Figure 13 shows the relationship between iteration times and the difference of contact stresses between the boundary nodes of meshes in the case of the simple-shaped model. The result indicated that the difference of stress decreased with increasing iteration times. Figure 14 shows reaction forces with and without mesh-mesh interaction in the case of the simple-shaped model. The result indicated the difference of reaction forces with considering the mesh-mesh interaction.

Next, the computation time for the new boundary setting was measured when the number of nodes of the cubic mesh was changed. Table 3 shows number of the triangles of the new boundary, inside triangles of the mesh, and the ratio of the triangles of the new boundary among the inside triangles, when number of the nodes of the cubic mesh is increased. Figure 15 shows the increase of number of triangles of the new boundary and calculation time for definition of the new boundary. The new boundary setting takes several seconds. Thus, it is not a real-time computation. However, the improvement of the algorithm and pre-processing would achieve real-time computation in the future.

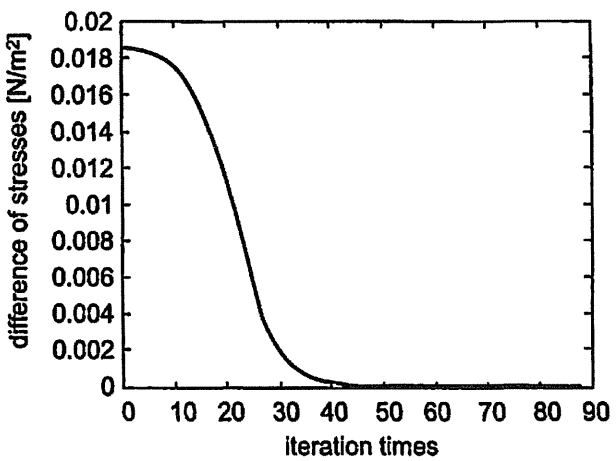

Fig. 13. Relationship between iteration times of interaction calculation and the difference of contact stresses

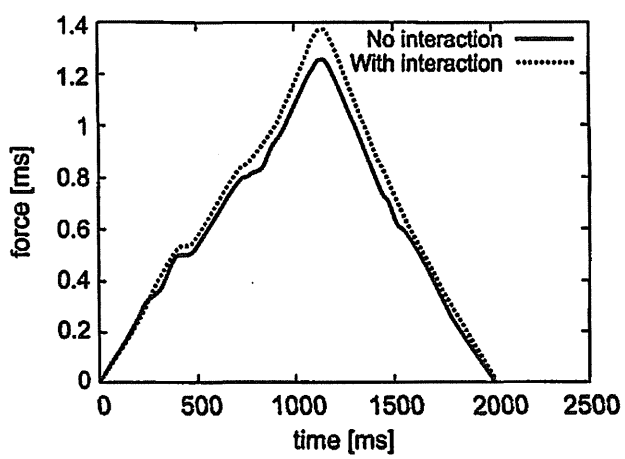

Fig. 14. Reaction forces with or without considering of interaction calculation

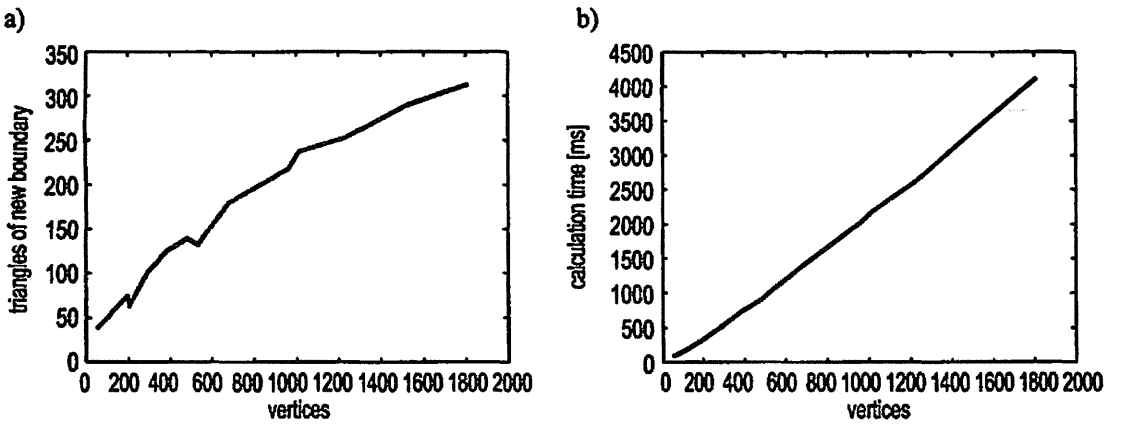

Fig. 15. Number of triangles of the new boundary and calculation time: (a) triangles of new boundary, (b) calculation time for definition of the new boundary

Table 3. Time for defining a new boundary

Vertices	50	107	124	195	207	291	386	483
Triangles of new boundary	38	51	57	74	64	100	125	139
Inside triangles	454	1232	1471	2448	2581	4013	5564	6937
Calculation time [ms]	83.6	169.5	194.6	323.0	345.1	518.9	731.4	902.5
Ratio [%]	8.4	4.1	3.9	3.0	2.5	2.5	2.2	2.0

Vertices	535	678	966	1013	1227	1521	1812
Triangles of new boundary	132	179	218	237	252	289	313
Inside triangles	8043	10719	15734	16863	20549	26415	32250
Calculation time [ms]	1035.3	1385.8	2029.5	2166.0	2627.0	3392.9	4116.6
Ratio [%]	1.6	1.7	1.4	1.4	1.2	1.1	1.0

Figure 16 shows the images produced by the developed system. The images show the early stage of the surgical approach in neurosurgery. The system allows user to exclude brain tissue interactively with force feedback. In Figure 16(a), a part of cerebellum is visible through a hole of the skull, and accessible by a virtual tool. In Figure 16(b), cerebellum is excluded by the virtual tool, which changes color from gray to red according to the magnitude of the reaction force. The color is set according to the formula: $(R, G, B) = (min(0.2 + f, 1), max(0.2 - f, 0), max(0.2 - f, 0))$, where f is the magnitude of the reaction force. Here, each color has the value ranged from 0 to 1. In Figure 16(c), (d), the skull is not visualized in the images.

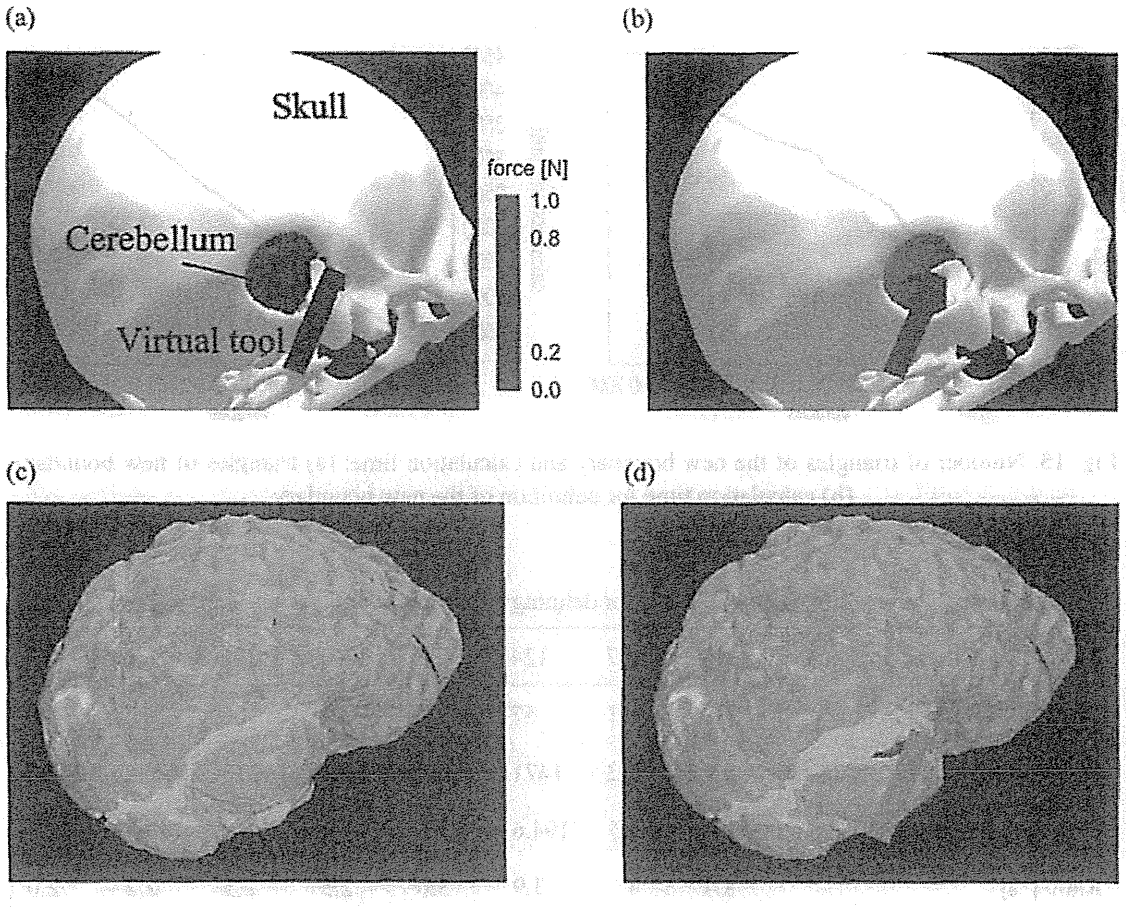

Fig. 16. Simulation result with brain meshes: (a) a part of cerebellum is visible through a hole of the skull, and accessible by a virtual tool, (b) cerebellum is excluded by the virtual tool, which changes color from gray to red according to the magnitude of the reaction force, and (c),(d) the skull is not visualized in the images

4. Conclusions

This paper proposed a FEM-based mesh-mesh interaction method with the multimodal 3D meshes. The proposed method detected an overlapped region between the meshes and defined a new boundary to consider interaction between the colliding meshes. The result of the simulation indicated that the proposed method enabled definition of the new boundary between the meshes and consideration of the mesh-mesh interaction by using simple and patient datasets. The force feedback system was implemented, and applied to the early stage of the surgical approach in neurosurgery. The results showed the real-time simulation of brain tissue deformation with visual and force feedback. As a future work, the simulation of a viscoelastic tissue model and a spinal fluid model would be integrated in the system.

Acknowledgment

This study was partly supported by Grant-in-Aid for Scientific Research (S16100001) from JSPS, the Global COE Program "*in silico* medicine" at Osaka University, and Casio science promotion foundation. This study was approved by the ethical committee of School of Medicine, Asahikawa Medical University (approval number: 694).

References

1. Liu A., Tendick F., Cleary K., Kaufmann C.: A survey of surgical simulation: applications, technology, and education. Presence: Teleoper. Virtual Environ, MIT Press, 2003, 12, 6, 599–614.
2. Sorensen T.S., Mosegaard J.: Haptic feedback for the GPU-based surgical simulator. Stud. Health Technol. Inform. 2006, 119, 523–528.
3. Kuroda Y., Hirai M., Nakao M., Sato T., Kuroda T., Nagase K., Yoshihara H.: Organ Exclusion Simulation with Multi-finger Haptic Interaction for Open Surgery Simulator. Stud. Health Technol. Inform. 2007, 125, 244–249.
4. Bachofen D., Zatonyi J., Harders M., Szekely G., Frueh P., Thaler M.: Enhancing the Visual Realism of Hysteroscopy Simulation. Medicine Meets Virtual Reality 2006, 31–36.
5. Kamada K., Ota T., Kawai K., Kuroda Y., Oshiro O., Aoki S., Saito N.: Visualization of cranial nerves and surrounding structures with a 3T-MR scanner for skull base surgery. Proc. Asian Australasian Congress of Neurosurgical Surgeon 2007, M19-4-6.
6. Malone H., Syed O., Downes M., D'Ambrosio A., Quest D., Kaiser M.: Simulation in Neurosurgery: A Review of Computer-Based Simulation Environments and Their Surgical Applications. Neurosurgery 2010, 67, 4, 1105–1116.
7. Hayashi N., Endo S., Shibata T., Ikeda H., Takaku A.: Neurosurgical simulation and navigation with threedimensional computer graphics. Neurol. Res. 1999, 21, 1, 60–66.
8. Spicer M.A., Apuzzo M.L.: Virtual Reality Surgery: Neurosurgery and the Contemporary Landscape. Neurosurgery 2003, 52, 3, 489–498.
9. Spicer M.A., van Velsen M., Caffrey J.P., Apuzzo M.L.: Virtual Reality Neurosurgery: A Simulator Blueprint. Neurosurgery 2004, 54, 4, 783–798.
10. Kuroda Y., Kamada K., Kagiyama Y., Imura M., Oshiro O.: Mesh Fusion Modeling for Neurosurgery Force Feedback System. Lecture Notes of the ICB Seminars: 10th Japanese-Polish Seminar on Biomedical Engineering: New Trends in biomedical and clinical engineering, 2010, 84, 97–102.
11. Kuroda Y., Kamada K., Kagiyama Y., Imura M., Oshiro O.: Neurosurgery Simulation with Multiple Meshes. Jap. J. Med. Virt. Real. 2010, 8, 1, 1–10 (in Japanese).
12. Kuroda Y., Nakao M., Kuroda T., Oyama H., Komori M.: Interaction Model between Elastic Objects for Haptic Feedback considering Collisions of Soft Tissue. Comp.r Meth. Progr. Biomed. 2005, 80, 3, 216–224.
13. Delingette H.: Toward realistic soft tissue modeling in medical simulation. Proc. IEEE 1998, 86, 3, 512–523.
14. Monserrat C., Meier U., Alcaniz M., Chinesta F., Juan M.C.: New approach for the real-time simulation of tissue deformations based on boundary element methods. Comput. Meth. Program. Biomed. 2001, 64, 2, 77–85.
15. Selle A., Su J., Irving G., Fedkiw R.: Robust High-Resolution Cloth Using Parallelism, History-Based Collisions, and Accurate Friction. IEEE Trans. Visual. Comp. Graph. 2009, 15, 2, 339–350.

16. Sibille L., Teschner M., Srivastava S., Latombe J.: Interactive simulation of the human hand. Proc. f Comput. Assist. Radiol. Surg. 2002, 7–12.
17. Joukhadar A., Wabbi A., Laugier C.: Fast contact localization between deformable polyhedra in motion. Proc. IEEE Comput. Animat. Conf. 1996, 126–135.
18. Hirota K., Kaneko T.: Haptic Representation of Elastic Objects. MIT Presence, 2001, 10, 5, 525–536, 2001.
19. Nakao M., Kuroda T., Minato K.: Volumetric Mask and its Real-time Processing for Volume Interaction. Trans. Virtual Reality Society of Japan 2005, 10, 4, 591–598 (in Japanese).